Shape effects

DOI: 10.1002/ange.200705828

# Shape and Crystal-Plane Effects of Nanoscale Ceria on the Activity of Au-$CeO_2$ Catalysts for the Water–Gas Shift Reaction**

*Rui Si and Maria Flytzani-Stephanopoulos**

The water–gas shift (WGS) reaction ($CO + H_2O \rightleftarrows CO_2 + H_2$) plays an important role in fuel processing for polymer electrolyte membrane (PEM) fuel-cell applications. The hydrogen in the reformate gas is upgraded by removal of the carbon monoxide, which is a strong poison of the anode catalysts in current PEM fuel cells. Active shift catalysts that are also stable under the operating conditions of practical fuel-cell systems are under intense study,[1] and nanostructured Au-$CeO_2$, first reported by Fu et al. as a promising low-temperature shift catalyst,[2] holds a prominent position. This catalyst exploits the strong interaction of ceria with finely dispersed and stabilized gold atoms and clusters on the surface of ceria.[3] Gold nanoparticles and clusters that interact strongly with oxide supports were first described by Haruta et al.[4] to be extremely active CO oxidation catalysts. Numerous studies since then have reaffirmed the activity of well-dispersed gold for CO oxidation and many other reactions. While a full mechanism of this catalytic process still needs to be established, even for the simplest of these reactions (CO oxidation), a careful investigation of the reported strong metal–support interaction through structural studies may provide further mechanistic insights as well as rationalize the design of practical catalysts. For the WGS reaction on Au-$CeO_2$, the importance of nanoscale ceria as a support that stabilizes active gold species has been demonstrated recently.[2,3,5–9]

Hydrolysis methods for the synthesis of ceria nanocrystals have proven to be powerful for controlling particle size[10] and crystal shape.[11–13] For example, Yan et al. have obtained single-crystalline $CeO_2$ nanopolyhedra ({111} and {100}), nanorods ({110} and {100}), and nanocubes ({100}) by hydrolysis of cerium(III) salts, combined with a hydrothermal treatment, and have further found that oxygen storage takes place both at the surface and in the bulk for nanorods and nanocubes but is restricted to the surface for nanopolyhedra, just like its bulk ceria counterpart.[12] Trovarelli et al. have studied the rearrangement of $CeO_2$ crystallites under aging and the exposure of more reactive {100} surfaces for CO oxidation.[13]

Very little is known for Au-$CeO_2$ composite polycrystalline nanomaterials with respect to the shape/crystal plane effect of $CeO_2$ on the gold species' activity/stabilization as highly active catalysts for the WGS reaction.[9] Herein, we present activity correlations with the shape (rod, cube, polyhedron) and crystal plane of nanoscale ceria as a support for gold catalysts for this reaction. The interaction between deposited gold and different crystal orientations is investigated at ambient pressure and monitored by several analytical techniques, including transmission electron microscopy (TEM), high-resolution TEM (HRTEM), X-ray photoelectron spectroscopy (XPS), and temperature-programmed reduction by hydrogen ($H_2$-TPR).

Figure 1 depicts our two-step preparation process, which includes hydrothermal synthesis of ceria nanorods, nanocubes, and nanopolyhedra[12] and the sequential introduction of gold by a deposition/precipitation (DP) method.[14] The bulk metal composition was determined by inductively coupled plasma atomic emission spectrometry (ICP-AES, Perkin–Elmer, Plasma 40). Table 1 shows that the attained Au concentration (0.8–0.9 atom%) is very close to the expected value (1 atom%) for each sample, which confirms the effectiveness of this DP method for depositing gold on a ceria surface. The powder X-ray diffraction (XRD, Rigaku RU300, $Cu_{K\alpha}$) patterns (see the Supporting Information) show only the face-centered cubic (*fcc*) structure of $CeO_2$ (space group: *Fm*3*m*) without any Au phase at around 38° or 44°, and the TEM (JEOL, 200cx) images in Figure 2 show that these three differently shaped ceria nanoparticles maintain

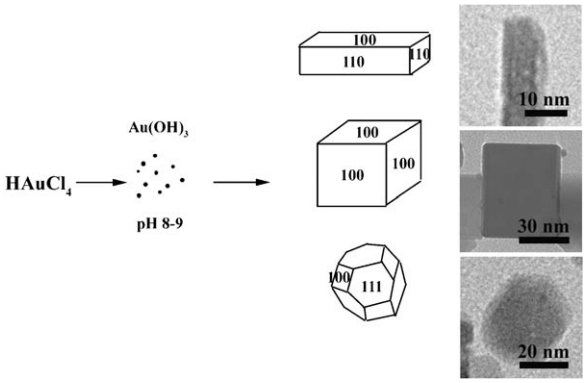


***Figure 1.*** Two-step synthesis of Au on $CeO_2$ nanorods, -cubes, and -polyhedra. The nanoscale ceria was prepared by a controlled hydrothermal technique.

[*] Dr. R. Si, Prof. M. Flytzani-Stephanopoulos
Chemical and Biological Engineering
Tufts University
4 Colby Street, Medford, MA 02155 (USA)
Fax: (+1) 617-627-3991
E-mail: maria.flytzani-stephanopoulos@tufts.edu

[**] Grant support from the DOE/BES-Hydrogen Fuel Initiative program (DE-FG02-05ER15730) and the NSF-NIRT program (grant 0304515) is gratefully acknowledged.

Supporting information for this article is available on the WWW under http://www.angewandte.org or from the author.

***Table 1:*** Gold loading, particle size (*D*), and XPS Au 4f peak analyses for Au on $CeO_2$ nanorods, -cubes, and -polyhedra.

| Sample | Au [atom %][a] | *D* [nm][b] | XPS Au 4f peak[c] | | | |
|---|---|---|---|---|---|---|
| | | | Au [atom %][d] | $Au^0$ | $Au^+$ | $Au^{3+}$ |
| Rods | 0.9 (0.5[e]) | (10.1±2.8) × (50–200) | 0.9 | – | 86.2% | 13.8% |
| Cubes | 0.9 (0.03[e]) | 29.5 ± 10.6 | 1.1 | 77.2% | 16.9% | 5.9% |
| Polyhedra | 0.8 (0.4[e]) | 11.0 ± 2.1 | 0.8 | 3.8% | 85.5% | 10.7% |

[a] Determined by ICP-AES. [b] Calculated for about 100 nanoparticles from the HRTEM images. [c] The binding energy was calibrated to the C 1s peaks at 285.0 eV. [d] Determined from Au 4f and Ce 3d cores in the XPS spectra. [e] After NaCN leaching at room temperature (pH 12) with addition of NaOH and oxygen sparging of the aqueous solution.[3]

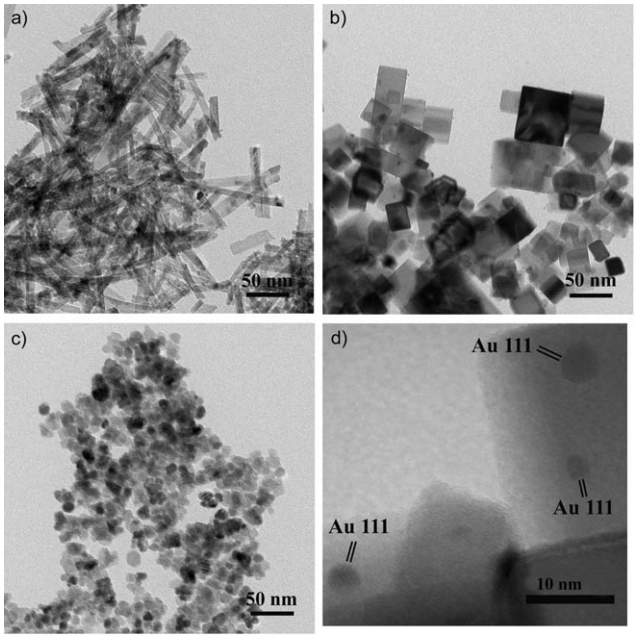


***Figure 2.*** TEM (a–c) and HRTEM (d) images of 1% Au on $CeO_2$ nanorods (a), -cubes (b, d), and -polyhedra (c).

their original crystal shapes after gold deposition—the $CeO_2$ nanorods display a uniform width of (10.1 ± 2.8) nm with a length of 50–200 nm (Figure 2a, Table 1), the $CeO_2$ nanocubes have a side-size of (29.5 ± 10.6) nm (Figure 2b, Table 1), and the $CeO_2$ nanopolyhedra have a diameter of (11.0 ± 2.1) nm (Figure 2c, Table 1). The HRTEM (JEOL, 2010) data allowed us to determine the exposed crystal planes for the different $CeO_2$ nanostructures. In agreement with Yan et al.,[12] they are {110} and {100} for the nanorods, {100} for the nanocubes, and {111} and {100} for the nanopolyhedra. Noticeably, a few nanocrystals with a particle size of about 3 nm can be identified by HRTEM as the gold phase of the gold catalyst on the ceria nanocubes (Figure 2d). No such gold nanoparticles were found for the rod and polyhedron samples.

The XPS (Axis Ultra, $Al_{K\alpha}$) data listed in Table 1 show that the surface Au concentrations (0.8–1.1 atom%) are in good agreement with those in the bulk (0.8–0.9 atom%), which means that the introduced gold species remain mostly on the surface or within the sub-surface layers of $CeO_2$. The high-resolution XPS spectra (Figure 3) show a distinct binding-energy shift of the Au 4f peaks between the rod/polyhedron and the cube samples. A peak-fitting procedure (see the Supporting Information) shows that ionic gold ($Au^+$ and $Au^{3+}$) is the main species in the rod or polyhedron samples while metallic gold ($Au^0$) is dominant in the ceria nanocubes.

We also used $H_2$-TPR to study the reducibility of surface oxygen

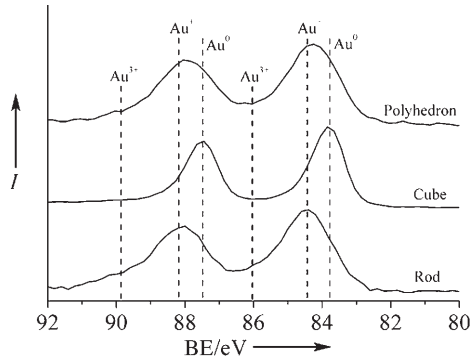


***Figure 3.*** Au 4f XPS spectra of 1% Au on $CeO_2$ nanorods, -cubes, and -polyhedra.

in each Au-$CeO_2$ catalyst. Figure 4 shows that the reduction of oxygen on the gold-ceria nanorods peaks at around 94 °C with an $H_2$ consumption of 753 μmol $g^{-1}$. According to our previous research, this reduction peak is due to the weakening of the Ce–O bond by strongly bound gold species.[2,8,15] Surface oxygen reduction peaks at 82 °C for the polyhedron sample, with a smaller hydrogen consumption of 425 μmol $g^{-1}$, whereas no obvious reduction peak appears up to 300 °C for the cube sample, thereby indicating its non-reducible nature at low temperatures, probably because of negligible interaction with the gold nanoparticles.

Weakly bound gold species were removed from the ceria surfaces by NaCN leaching.[3] For the rod and polyhedron samples, 0.5 and 0.4 atom% gold was retained after leaching, respectively (Table 1), whereas for the cube sample only

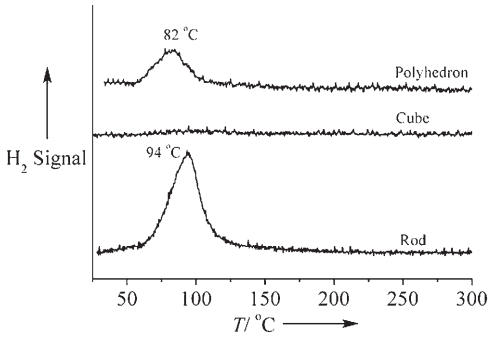


***Figure 4.*** $H_2$-TPR profiles of the 1% Au on $CeO_2$ nanorods, -cubes, and -polyhedra.

0.03 atom% gold remained. These results are consistent with the XPS and $H_2$-TPR findings, which showed that a much higher fraction of strongly bound gold species is present on the surface of the $CeO_2$ nanorods or -polyhedra than on the nanocubes.

The relationship between the catalytic activity and the structural/surface properties of the Au-$CeO_2$ system was investigated by performing the WGS reaction. The "light-off" WGS reaction profiles in Figure 5 allow the activity of the

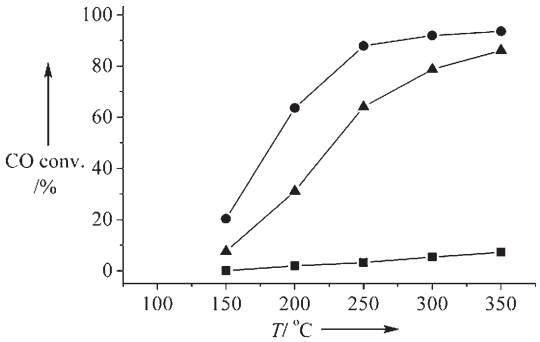


***Figure 5.*** WGS reaction "light-off" profiles for 1% Au on $CeO_2$ nanorods (●), -cubes (■), and -polyhedra (▲).

three catalysts to be ranked as: rod > polyhedron ≫ cube. The CO conversion over the rod sample is close to 100% (approx. 90%) at 250°C, whereas the cube sample shows only around 20% CO conversion at 350°C. We also compared the reaction rates of $CO_2$ produced by these gold-ceria catalysts. Again, the rod sample shows the highest value of 2.4 μmol $g_{cat.}^{-1} s^{-1}$ at 150°C, followed by the polyhedron one (0.9 μmol $g_{cat.}^{-1} s^{-1}$). The cube sample produces no $CO_2$ at 150°C and shows a reaction rate of 0.8 μmol $g_{cat.}^{-1} s^{-1}$ at 350°C.

Since the DP conditions (base, pH value, aging and calcination temperature, time, etc.) were kept the same for these gold-ceria samples, the above differences must originate from the nature of the support itself. The nanosize effect of ceria should be considered first as this is known to improve its intrinsic reducibility and formation of oxygen vacancies upon spontaneous reduction of $Ce^{4+}$ to $Ce^{3+}$.[16,17] The ceria particle sizes obtained in our synthesis are 10–30 nm, which is above the reported critical size for the small size effect in $CeO_2$ (10–15 nm).[16,17] We also calculated the specific surface areas ($S$) of typical $CeO_2$ crystal planes ({100}, {110}, and {111}) based on the corresponding geometric shape, particle size (from HRTEM), and the real density (from XRD). The $S_{100}$ and $S_{110}$ values for the ceria nanorods are both around 27 $m^2 g^{-1}$, which is the same as for the nanocubes. The sum of $S_{100}$ and $S_{111}$ for the $CeO_2$ nanopolyhedra is about 75 $m^2 g^{-1}$, which means that these three $CeO_2$ materials are comparable even though the nanocube side (approx. 30 nm) is much longer than the width of the nanorod (approx. 10 nm) or the diameter of the nanopolyhedron (approx. 11 nm).

Theoretical studies have shown that the formation energy of anion vacancies for different $CeO_2$ surfaces follows the order {110} < {100} < {111},[18] which means that oxygen vacancies, which are indispensable for stabilizing metals, are easier to form on the $CeO_2$ {110} planes. Therefore, compared with ceria nanocubes ({100}) and nanopolyhedra ({100} and {111}), ceria nanorods ({110} and {100}) should be better supports for anchoring and dispersing very fine gold clusters. This would explain why gold is dispersed and stabilized more effectively on the $CeO_2$ nanorods, which, in turn, leads to a higher reducibility and activity of the Au-$CeO_2$ surface for the WGS reaction. According to the above formation-energy sequence, ceria nanocubes enclosed by pure {100} planes should be a better support for gold than nanopolyhedra ({111} and {100} mixed). However, the $CeO_2$ {100} plane is a polar surface, composed of positively charged Ce layers and negatively charged O layers. This unique structure is not stable upon heating and will relax to a low-energy surface.[19] We therefore analyzed the microstrain in the $CeO_2$ lattice, which is mainly caused by defects (kinks, steps, dislocations, vacancies, etc.), from the XRD data. Table 2 shows that the

***Table 2:*** Lattice microstrain ($\varepsilon$) of different crystal planes of the $CeO_2$ and Au-$CeO_2$ nanorods, -cubes, and -polyhedra.

| Sample | $\varepsilon$[a] [%] | | |
|---|---|---|---|
| | (111) | (200) | (220) |
| $CeO_2$ rods | 1.1 | 1.3 | 0.9 |
| $CeO_2$ cubes | 0.3 | 0.2 | 0.2 |
| $CeO_2$ polyhedra | 0.9 | 0.6 | 0.5 |
| Au-$CeO_2$ nanorods | 0.8 | 0.8 | 0.9 |
| Au-$CeO_2$ nanocubes | 0.2 | 0.3 | 0.2 |
| Au-$CeO_2$ nanopolyhedra | 0.7 | 0.6 | 0.5 |

[a] Estimated by the single-line method from analysis of XRD line broadening using a pseudo-Voigt profile function.[24]

nanorod sample has the highest lattice strain both before and after gold deposition. The polyhedron sample follows, while the nanocube sample is the least strained. The lattice strain therefore correlates with the activity in the present system, as has been reported for other systems recently.[20–23]

In summary, we have prepared gold-ceria catalysts by depositing gold on the different facets of ceria nanorods, nanocubes, and nanopolyhedra in a two-step process that involves controlled hydrothermal synthesis of the cerium oxide shapes followed by deposition/precipitation of gold. A strong shape/crystal plane effect of $CeO_2$ on the gold-ceria activity for the WGS reaction has been identified. The rod-like ceria enclosed by {110} and {100} planes is most active for gold stabilization/activation. These findings can be extended to new studies of other metal-oxide surfaces at normal pressures.

## Experimental Section

$Ce(NO_3)_3 \cdot 6H_2O$ (99.5%, Alfa; 4.5 mmol) was dissolved in aqueous NaOH solution (90 mL; 98%, Alfa) of the appropriate concentration ($C_{NaOH}$; see below). This stock solution was stirred at room temperature for 10 min in a Teflon bottle and then sealed tightly in a stainless-steel autoclave. Hydrothermal treatment was carried out at different temperatures ($T$) for 24 h. After cooling, the white precipitates obtained were collected, washed with deionized (DI) water, and dried in vacuo at 70–80°C overnight. The dried yellow powders were calcined in air at 400°C for 4 h. The values of $C_{NaOH}$ and $T$ were varied according to the target crystal shape (rod: $C_{NaOH} = 6$ M,

  

$T = 100\,°C$; cube: $C_{NaOH} = 6\,M$, $T = 180\,°C$; polyhedron: $C_{NaOH} = 0.1\,M$, $T = 180\,°C$).

$CeO_2$ powder (3 g) was slurried in DI water (150 mL) whilst stirring and aqueous $(NH_4)_2CO_3$ solution (75 mL; 1 M) was then added. $HAuCl_4 \cdot 3H_2O$ (99.99%, Alfa; 0.174 mmol) was dissolved in DI water (75 mL) and added to the above solution dropwise. The pH value was kept at 8–9 during the whole process. The resulting precipitate was aged at room temperature for 1 h, then filtered and washed three times with DI water at 60–70 °C. The product was dried in vacuo at 70–80 °C overnight and then calcined in air at 400 °C for 4 h. NaCN leaching was performed with an aqueous 2% NaCN/NaOH solution (pH 12) at room temperature.

$H_2$-TPR was carried out with a Micromeritics Pulse ChemiSorb 2705 instrument. The catalyst powders were pre-oxidized in a 20% $O_2$/He gas mixture at 350 °C for 30 min and the test was performed with a 20% $H_2/N_2$ gas mixture from room temperature to 300 °C (5 °C $min^{-1}$). The "light-off" measurements for the WGS reaction were conducted at atmospheric pressure with a loading of about 100 mg of catalyst powder. The reaction gas mixture was 2% CO/10% $H_2O$/He (70 mL $min^{-1}$). The feed and product gas streams were analyzed with a HP-6890 gas chromatograph (GC) equipped with a thermal conductivity detector.

Received: December 19, 2007
Published online: March 10, 2008

**Keywords:** cerium oxide · fuel cells · gold · materials science · surface chemistry

[1] W. Deng, M. Flytzani-Stephanopoulos, *Angew. Chem.* **2006**, *118*, 2343; *Angew. Chem. Int. Ed.* **2006**, *45*, 2285.
[2] Q. Fu, A. Weber, M. Flytzani-Stephanopoulos, *Catal. Lett.* **2001**, *77*, 87.
[3] Q. Fu, H. Saltsburg, M. Flytzani-Stephanopoulos, *Science* **2003**, *301*, 935.
[4] M. Haruta, N. Yamada, T. Kobayashi, S. Iijima, *J. Catal.* **1989**, *115*, 301.
[5] Q. Fu, W. Deng, H. Saltsburg, M. Flytzani-Stephanopoulos, *Appl. Catal. B* **2005**, *56*, 57.
[6] Q. Fu, S. Kudriavtseva, H. Saltsburg, M. Flytzani-Stephanopoulos, *Chem. Eng. J.* **2003**, *93*, 41.
[7] Z.-P. Liu, S. J. Jenkins, D. A. King, *Phys. Rev. Lett.* **2005**, *94*, 196102.
[8] W. Deng, J. De Jesus, H. Saltsburg, M. Flyzani-Stephanopoulos, *Appl. Catal. A* **2005**, *291*, 126.
[9] Z.-Y. Yuan, V. Idakiev, A. Vantomme, T. Tabakova, T.-Z. Ren, B.-L. Su, *Catal. Today* **2008**, *131*, 203.
[10] Y.-W. Zhang, R. Si, C.-S. Liao, C.-H. Yan, C.-X. Xiao, Y. Kou, *J. Phys. Chem. B* **2003**, *107*, 10159.
[11] K. Zhou, X. Wang, X. Sun, Q. Peng, Y. Li, *J. Catal.* **2005**, *229*, 206.
[12] H.-X. Mai, L.-D. Sun, Y.-W. Zhang, R. Si, W. Feng, H.-P. Zhang, H.-C. Liu, C.-H. Yan, *J. Phys. Chem. B* **2005**, *109*, 24380.
[13] E. Aneggi, J. Llorca, M. Boaro, A. Trovarelli, *J. Catal.* **2005**, *234*, 88.
[14] S. Tsubota, M. Haruta, D. Cunningham, Y. Bando, *Preparation of Catalysts VI* **1991**, 227.
[15] W. Deng, C. Carpenter, N. Yi, M. Flytzani-Stephanopoulos, *Top. Catal.* **2007**, *44*, 199.
[16] X.-D. Zhou, W. Huebner, *Appl. Phys. Lett.* **2001**, *79*, 3512.
[17] F. Zhang, S.-W. Chan, J. E. Spanier, E. Apak, Q. Jin, R. D. Robinson, I. P. Herman, *Appl. Phys. Lett.* **2002**, *80*, 127.
[18] T. X. T. Sayle, S. C. Parker, D. C. Sayle, *Phys. Chem. Chem. Phys.* **2005**, *7*, 2936.
[19] M. Baudin, M. Wójcik, K. Hermansson, *Surf. Sci.*, **2000**, *468*, 51.
[20] R. Si, Y.-W. Zhang, S.-J. Li, B.-X. Lin, C.-H. Yan, *J. Phys. Chem. B* **2004**, *108*, 12481.
[21] N. Yi, Y. Cao, Y.-M. Liu, W.-L. Dai, H.-Y. He, K.-N. Fan, *Chem. Lett.* **2005**, *34*, 108.
[22] X. Wang, J. A. Rodriguez, J. C. Hanson, D. Gamarra, A. Martínez-Arias, M. Fernández-García, *J. Phys. Chem. B* **2005**, *109*, 19595.
[23] I. Kasatkin, P. Kurr, B. Kniep, A. Trunschke, R. Schlögl, *Angew. Chem.* **2007**, *119*, 7465; *Angew. Chem. Int. Ed.* **2007**, *46*, 7324.
[24] T. H. de Keijser, J. I. Langford, E. J. Mittemeijer, A. B. P. Vogels, *J. Appl. Crystallogr.* **1982**, *15*, 308.

  